TISSUE ENGINEERING: Part A
Volume 28, Numbers 1 and 2, 2022

DOI: 10.1089/ten.tea.2021.0064

termis
Tissue Engineering
& Regenerative Medicine
International Society

ORIGINAL ARTICLE

Adipogenic Differentiation Alters Properties of Vascularized Tissue-Engineered Skeletal Muscle

Francisca M. Acosta, PhD,[1,2,i] Kennedy K. Howland, BS,[1] Katerina Stojkova, MS,[1] Elizabeth Hernandez,[1] Eric M. Brey, PhD,[1] and Christopher R. Rathbone, PhD[1]

Advances in the engineering of comprehensive skeletal muscle models *in vitro* will improve drug screening platforms and can lead to better therapeutic approaches for the treatment of skeletal muscle injuries. To this end, a vascularized tissue-engineered skeletal muscle (TE-SkM) model that includes adipocytes was developed to better emulate the intramuscular adipose tissue that is observed in skeletal muscles of patients with diseases such as diabetes. Muscle precursor cells cultured with and without microvessels derived from adipose tissue (microvascular fragments) were used to generate TE-SkM constructs, with and without a microvasculature, respectively. TE-SkM constructs were treated with adipogenic induction media to induce varying levels of adipogenesis. With a delayed addition of induction media to allow for angiogenesis, a robust microvasculature in conjunction with an increased content of adipocytes was achieved. The augmentation of vascularized TE-SkM constructs with adipocytes caused a reduction in maturation (compaction), mechanical integrity (Young's modulus), and myotube and vessel alignment. An increase in basal glucose uptake was observed in both levels of adipogenic induction, and a diminished insulin-stimulated glucose uptake was associated with the higher level of adipogenic differentiation and the greater number of adipocytes.

Keywords: skeletal muscle, tissue engineering, microvessel, adipose

Impact Statement

The findings of the current study represent the effectiveness of employing a combinatorial approach involving muscle precursor cells and microvascular fragments to create a vascularized tissue-engineered skeletal muscle model with adipocytes that induce structural and metabolic changes. This model is a platform to support the discovery of mechanisms underlying the phenomena of intramuscular adipose tissue that is characteristic of the skeletal muscles of patients with diseases.

Introduction

The continued development of strategies to engineer skeletal muscle tissues *in vitro* that emulate the cellular heterogeneity that exists *in vivo* can lead to more comprehensive skeletal muscle models for drug discovery, disease modeling, treatments for injuries, and research into the cell-to-cell interactions that exist within skeletal muscle.[1–5] The use of induced pluripotent stem cells to create a complex system containing myogenic cells, vascular endothelial cells, pericytes, and motor neurons into a single construct exemplifies this concept.[6] The modeling of skeletal muscle diseases, where deficits in cell-to-cell signaling contribute to poor physiological outcomes, is one example where the sustained advancement toward complex multicellular models can be beneficial.

One of the characteristics of skeletal muscle that is present in a number of pathologies, but has received relatively little attention and is rarely incorporated in strategies to tissue engineer skeletal muscle, is the presence of intramuscular adipose tissue (IMAT; fat located between muscle fibers and beneath the muscle fascia).[7–10] Detrimental metabolic consequences and diminished muscle function are a few of the negative consequences that are associated with IMAT. As an example, an interesting characteristic of diabetic skeletal muscle is an increased infiltration of adipose

[1]Department of Biomedical Engineering and Chemical Engineering, University of Texas at San Antonio, San Antonio, Texas, USA.
[2]UTSA-UTHSCSA Joint Graduate Program in Biomedical Engineering, San Antonio, Texas, USA.
[i]ORCID ID (https://orcid.org/0000-0002-0171-9901).

tissue that is associated with increased insulin resistance.[10] In addition, adipose tissue infiltration within skeletal muscle is also associated with aging and reduced contractile function.[11,12] Skeletal muscles of patients with Duchenne muscular dystrophy can also be characterized by a high level of fat infiltration.[13] The mechanisms involved in the cross talk between adipocytes and muscle cells that contribute to negative physiological outcomes have not been fully resolved; however, studies investigating the cross talk between adipocytes and muscle cells, especially in the context of obesity and type 2 diabetes, support the idea that communication between them contributes to metabolic dysfunction.[14,15]

The formation of vascularized engineered skeletal muscle tissues can more comprehensively evaluate IMAT in skeletal muscle *in vitro* as it will allow for cross talk between myogenic cells, adipocytes, and the microvasculature. This is especially true when taking into consideration that under conditions where IMAT is increased, such as diabetes, deficits in the microvasculature are also observed.[10,16,17] The idea that the microvasculature is affected by adipocytes is supported by the observation that adipose tissue derived from obese/insulin-resistant subjects is associated with a reduced capillary density.[18] In the context of lipid-induced insulin resistance, muscle cells have been shown to transmit exosomes with downstream effects both within and beyond skeletal muscle.[19] In diseased skeletal muscle, vascular integrity is compromised; the myogenic cell-derived diseased skeletal muscle has diminished function that includes an impaired ability to influence angiogenesis.[20–24] Levy *et al.*[25] demonstrated that myogenic cells derived from diabetic patients secrete elevated amounts of interleukin 8; this outcome resulted in impaired stimulation of angiogenesis. Conversely, endothelial cells have the ability to secrete factors that can enhance myogenic cell growth.[26] Similarly, one mechanism contributing to the influence of the microvasculature on myogenesis may involve the control of muscle stem cells by endothelial cell-derived Notch ligand Dll4.[27] Collectively, there are a large number of interactions between myogenic cells, adipocytes, and microvessels that can contribute to the manifestation of diseases such as diabetes. While the interaction between adipocytes and myogenic cells has been previously evaluated in models *in vitro*,[14,28,29] it is prudent to include a microvasculature to provide a more comprehensive model for evaluating skeletal muscle disease.

Given the critical role of the microvasculature in skeletal muscle homeostasis, much effort has been directed toward creating vascularized tissue-engineered skeletal muscle (TE-SkM). One popular strategy for the vascularization of TE-SkM *in vitro* has focused on the introduction of endothelial cells along with an array of supporting cells into the TE-SkM.[30] A large body of work has demonstrated that biomaterial selection, mechanical stimulation, and growth factor application are important considerations in the design of vascularized TE-SkM.[30,31] A limitation to many of these approaches is that there is a high degree of *in vitro* manipulation required to recapitulate the intricacies of the vasculature. Conversely, a more direct approach to the vascularization of scaffolds involves the use of microvessels from adipose tissue called microvascular fragments (MVFs).[32] MVFs have been demonstrated to successfully vascularize a variety of scaffolds for the purpose of improving tissue perfusion *in vivo*, as well as providing a more physiological means of microvascular assessments *in vitro*.[33–38] The benefits of using an MVF-based approach to achieve scaffold vascularization may be obvious, but their utility for generating an engineered tissue containing both a vasculature and adipocytes may be less apparent. In this regard, the presence of resident precursor cells within the MVFs that have adipogenic potential is an especially important characteristic of MVFs that can be exploited to generate an engineered tissue that contains both a vasculature and adipocytes.[34,38,39] Collectively, the vascularizing potential of MVFs coupled with their potential to provide adipogenic cells makes them a unique tool to generate engineered skeletal muscle for better understanding skeletal muscle dynamics.

Engineered skeletal muscles containing adipocytes that rely on the adipogenic differentiation of muscle precursor cells (MPCs) alone have been created,[40] and it has also been demonstrated that MVFs can be used as a source of microvessels in addition to adipocytes, even after the microvessels have gone through a period of angiogenic sprouting.[34] In the current study, MPCs were combined with MVFs to generate a vascularized TE-SkM with an even higher number of adipocytes while still maintaining a persistent vasculature. These efforts have resulted in the development of a more comprehensive system for skeletal muscle modeling, as well as providing a means to the system to better understand, and potentially treat skeletal muscle injuries and disease states.

Materials and Methods

Animals

Experiments were carried out using cells or microvessels isolated from 8- to 12-month-old male Lewis rats (Envigo, Indianapolis, IN). All animals were housed in a temperature-controlled environment with a 12-h light–dark cycle and fed *ad libitum*. This study was conducted in compliance with the Animal Welfare Act and the Implementing Animal Welfare Regulations, in accordance with the principles of the Guide for the Care and Use of Laboratory Animals, and was approved by the Institutional Animal Care and Use Committee at the University of Texas at San Antonio.

MPC isolation

Rat MPCs were isolated using the methods described in our previous studies.[40,41] Briefly, tibialis anterior, extensor digitorum longus, quadriceps, gastrocnemius, and plantaris muscles were minced, digested with protease type XIV, and filtered with a 100 μm Steriflip (Millipore, Burlington, MA) to remove debris. After differential centrifugation, and pre-plating, non-adherent MPCs were transferred to Matrigel-coated dishes and cultured in growth medium (GM) composed of 20% fetal bovine serum (FBS), 1% penicillin–streptomycin (P/S), 0.2% MycoZap (MZ), Dulbecco's modified Eagle medium (DMEM) with 1 g/L D-glucose, L-glutamine, and 110 mg/L sodium pyruvate. Experiments were conducted using TE-SkM constructs that contained MPCs (passage 2 or 3) derived from at least four separate animals.

MVF isolation

MVFs were isolated from the epididymal (EPI), inguinal (ING), and subcutaneous (SUBQ) fat depots similar to that previously described.[34] Briefly, adipose tissue from the EPI, ING, and SUBQ fat from 8- to 12-month-old male Lewis rats (Envigo, Huntingdon, United Kingdom) were subjected to an 8- to 15-min collagenase type I digestion (Worthington Biochemical Corporation, Lakewood, NJ) at 37°C with agitation. The digested tissue was subjected to centrifugation ($400\times g$, 4 min), which resulted in a floating layer of adipocytes and a pellet containing a heterogeneous mixture of cells and MVFs. The pellet was resuspended in phosphate-buffered saline (PBS) containing 0.1% bovine serum albumin (Sigma–Aldrich, St. Louis, MO) and filtered through 500 μm and 37 μm filters (Carolina Biological Supply, Burlington, NC) to remove large debris and minimize cell contamination, respectively. MVFs were then counted and centrifuged before resuspension in fibrinogen (Sigma–Aldrich) in DMEM (20 mg/mL) at a concentration of 20,000 MVFs/mL for TE-SkM formation.

TE-SkM formation and culture conditions

TE-SkMs were fabricated and created as we have described previously,[40] with the exception that MVFs were added. Briefly, polydimethylsiloxane (PDMS) molds in a half-pipe structure (final dimensions: $25\times4.7\times2.35$ mm; L × W × H) containing two small metal pins that acted as anchor points for the hydrogel constructs were coated with pluronic acid (10 mg/mL in PBS) for 48 h before seeding. After a PBS wash to remove the excess pluronic acid, MPCs (1.25×10^6 cells/mL) ± MVFs (20,000 MVFs/mL) were resuspended in fibrinogen previously solubilized in DMEM at the concentration of 20 mg/mL. Fibrin gels (5.7 mg/mL, 300 μL) were formed by mixing the cells resuspended in a fibrinogen solution with 10 U/mL of thrombin (2:5 part, respectively).

Constructs in the myogenic media (MM) groups were grown in myogenic GM (described in MPC isolation) for 4 days and then switched to myogenic differentiation media (DM; 2% horse serum, 1% P/S, 0.2% MZ, and DMEM) for 17 days. Samples in the adipogenic media (AM) groups were grown in myogenic GM for 4 days, switched to DM for 3 days, and then cultured in two different types of adipogenic DM: (1) Adipose induction media that consisted of DMEM/F12, 20% FBS, 1% P/S, 0.2% MZ, 10 μg/mL insulin, 10 μM forskolin, and 1 μM dexamethasone for 4 days, followed by maturation media containing DMEM/F12, 20% FBS, 1% P/S, 0.2% MZ, and 5 μg/mL insulin for 10 days (this group is referred to as MM/AM) or (2) Adipose induction media that was supplemented with 0.5 μM rosiglitazone (Rosi) and 1 nM triiodothyronine (T3), followed by a maturation media that consisted of AM maturation media supplemented with 1 μM Rosi and 1 nM T3 for an additional 10 days (this group is referred to as MM/AM+). Refer to Figure 1 for a schematic depicting the culture conditions used to accomplish the goals of these studies. All media throughout the study were supplemented with 1 mg/mL aminocaproic acid to prevent fibrinolysis. Under all culture conditions, the appropriate volume of medium (500 μL) was replaced every other day throughout the study, whereas cultures were maintained in a humidified incubator at 37°C and 5% carbon dioxide.

TE-SkM compaction analysis

The surface area coverage of the fibrin gels ($n=4$ per group) within the PDMS molds was monitored by taking daily images of the TE-SkM using a digital camera (Sony α600; Minato City, Tokyo, Japan). The percentage of compaction was determined through an evaluation of the ratio between the total area of the molds and the hydrogel's surface area. The analysis was carried out using the ImageJ (National Institutes of Health, Bethesda, MD).

Creatine kinase assay

TE-SkM construct creatine kinase (CK) activity was evaluated using a Creatine Kinase Activity Assay Kit (MAK116; Sigma–Aldrich) in accordance with the manufacturer's instructions. After lysing TE-SkMs ($n=4$ per group) with 1 × RIPA lysis buffer (EMD Millipore, 20–188, Billerica, MA) and tissue homogenization (Omni, Kennesaw, GA), samples were centrifuged ($15{,}000\times g$) to remove debris. Ten microliters of each sample was combined with 100 μL of reconstituted reagent containing the assay buffer, a substrate solution, and the enzyme mix. Samples were incubated at room temperature for 40 min before absorbance measurements were made (340 nm). CK measurements were normalized to protein content (determined using a BCA protein assay [EMD Millipore, Germany]).

Uniaxial tensile testing

TE-SkMs ($n=4$ per group) were stained with hematoxylin for 1 min, then rinsed with PBS five times for visualization, and then evaluated using uniaxial tensile testing until the point of failure with a 2.5 N load cell (Ustretch; CellScale, Waterloo, ON). The test was performed by elongating the samples (12 mm), stimulating them cyclically, and then to failure at 1 mm/s while water immersed at 37°C. BioQuant (Nashville, TN) was used to calculate the average sample width for the determination of the cross-sectional area of each sample. Mechanical parameters were calculated using the following formulas:

$$\textbf{\textit{Ultimate Tensile Strength}} = \textit{Ultimate Tensile Load}\,/\textit{Cross}-\textit{Sectional Area},$$

$$\textbf{\textit{Elongation at Failure}} = \textit{Elongation at Rupture}\,/\textit{Initial Length}\times100,$$

$$\textbf{\textit{Stiffness}} = \Delta F/\Delta l,$$

$$\textbf{\textit{Young's Modulus}} = \Delta\sigma/\Delta\varepsilon.$$

Histological analysis

After 2 h of fixation (room temperature) in 4% formaldehyde, TE-SkM samples ($n=4$ per group) were permeabilized using 0.5% Triton-X for 20 min, blocked using 10% goat serum for 2 h, and then stained using Rhodamine-labeled Griffonia (Bandeiraea) Simplicifolia Lectin I (GS-Lectin I; Vector Labs, Burlingame, CA, 1:100), borondipyrromethene (BODIPY; ThermoFisher, D3922, 1:100),

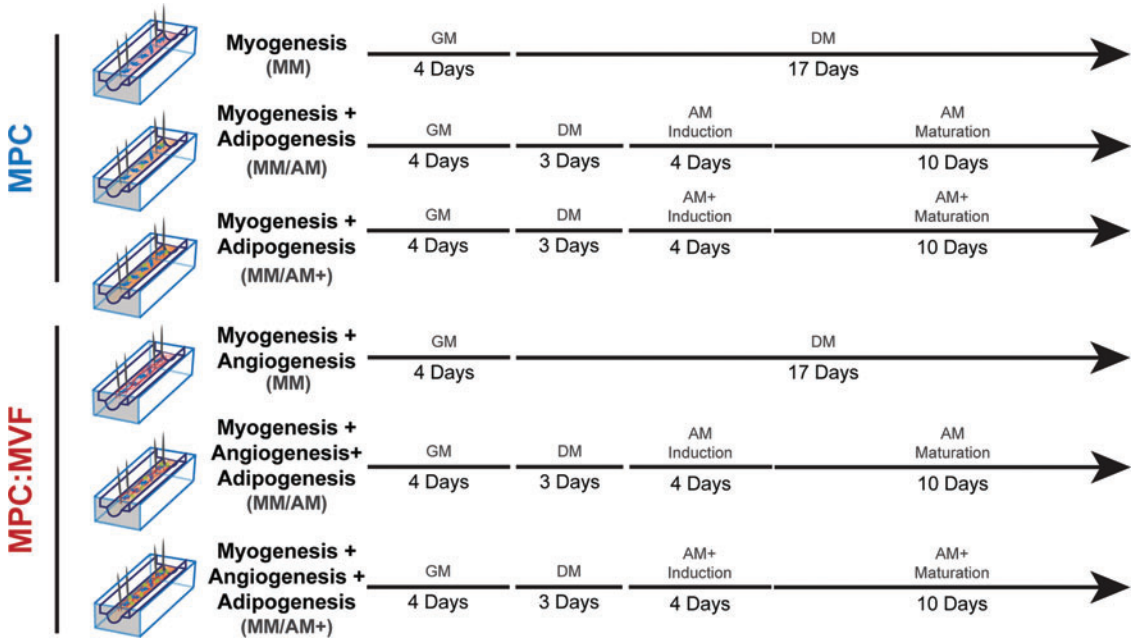

FIG. 1. Schematic describing the study. TE-SkM constructs containing MPC only or a combination of MPCs and MVFs (MPC:MVF) were treated with myogenic GM, myogenic DM, or two levels of adipogenic media (AM or AM+) for the time periods indicated. The *arrowhead* indicates the time at which the analysis was performed. AM, adipogenic media; DM, differentiation media; GM, growth media; MPC, muscle precursor cells; MVF, microvascular fragments; TE-SkM, tissue-engineered skeletal muscle. Color images are available online.

F-Actin (ThermoFisher, R37112), and DAPI (ThermoFisher, R37606). Three regions of interests (ROIs) (comprising ~50% of total construct length) per sample were imaged using a rendering of 30 µm thickness/3 µm sections (Leica TCS SP8 Confocal Microscope, Buffalo Grove, IL). BODIPY and Lectin quantification was performed using the Leica 3D analysis toolkit through Otsu thresholding. Additionally, the object count obtained through thresholding was graphed as a means of determining the connectivity of structures. The alignment of TE-SkM was quantified using both F-Actin and Lectin staining using the ImageJ directionality plugin.

Insulin-stimulated glucose uptake

TE-SkM samples ($n=6$ per group) were cultured in DMEM without serum or glucose for 24 h. Subsequently, samples were changed to DMEM ± insulin (1 mM) for 2 h, followed by the addition of 2-deoxyglucose (0.1 mM) for 1 h. Finally, a 2-deoxyglucose-6-phosphate (2DG6P) detection reagent was used to quantify the amount of glucose internalized by the cells (Glucose Uptake-Glo™ Assay; Promega, Madison, WI). Luminescence was measured after 2 h with a spectrophotometer (BioTek, Winooski, VT).

Gene expression analysis

TE-SkM samples ($n=4$ per group) were homogenized (Omni), and RNA was isolated and purified from TE-SkM using a Qiagen RNeasy Mini Kit (Valencia, CA) according to the manufacturer's guidelines. mRNA concentrations were measured (Take3 Micro-Volume Plate; BioTek) and then normalized to 150 ng of mRNA for its conversion to cDNA. Isolated RNA was converted to cDNA using the iScript cDNA Synthesis Kit (Bio-Rad, Hercules, CA). Real-time quantitative polymerase chain reaction (qPCR) was performed using a CFX96 Touch Real-Time PCR Detection System (Bio-Rad). The primers used to carry out the qPCR analysis were predesigned (Sigma–Aldrich; Supplementary Table S1). Ten microliters of iTaq Universal SYBR Green Supermix (Bio-Rad) was used for each reaction. Fold expression levels were calculated using the $2^{-\Delta\Delta Ct}$ method, where the MM/MM TE-SkMs were designated as the calibrator group, and glyceraldehyde-3-phosphate dehydrogenase (*GAPDH*) expression was used as the endogenous control.[42]

Statistical analysis

GraphPad Prism Software 6 (GraphPad Software, Inc., La Jolla, CA) was used to run one-way analysis of variance tests with Tukey's multiple comparison analyses to determine differences between groups. Statistical significance was determined when $p<0.05$. All results are presented as mean ± standard error of the mean.

Results

Maturation of TE-SkMs containing MPCs or a combination of MPCs and MVFs under different culture conditions

At the macroscopic level, all constructs appeared to be similar in size at the time of creation regardless of group or media condition (Fig. 2A). Overall, all groups exhibited an increase in compaction as demonstrated by a decrease in surface area over 21 days, with a greater increase in compaction in the MPC:MVF group compared with the MPC group (Fig. 2A). These visual observations were supported

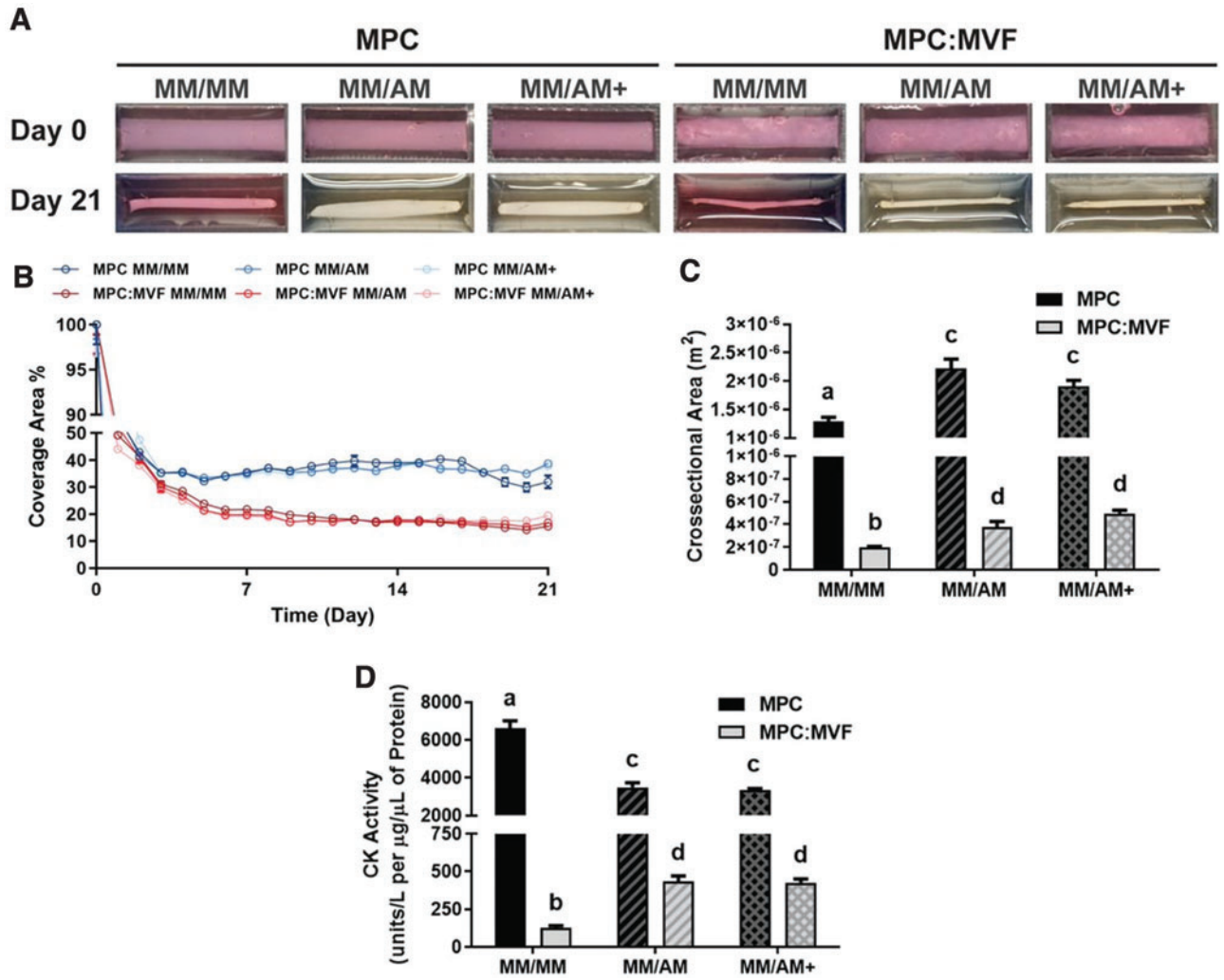

FIG. 2. TE-SkM characterization. TE-SkM constructs containing MPC only or a combination of MPCs and MVFs (MPC:MVF) were treated with MM only, or MM before two levels of adipogenic media (AM or AM+) ($n=4$ per group). **(A)** Representative images of the constructs after 0 or 21 days of culture. **(B)** Quantification of the change in the TE-SkM coverage area over time ($n=4$ per group). **(C)** Quantification of TE-SkM cross-sectional areas after 21 days of culture ($n=4$ per group). **(D)** Quantification of creatine kinase activities of TE-SkMs after 21 days of culture ($n=4$ per group). Results are reported as mean ± standard error. *Bars displaying different letters* are statistically significant from each other ($p<0.05$). *Bars with the same letters* are not significantly different ($p>0.05$). MM, myogenic media. Color images are available online.

by the quantification of the coverage area over the 21-day observation period (Fig. 2B) and the cross-sectional area on day 21 (Fig. 2C). More specifically, compaction was steady up to day 2 in all groups, although by days 3–4, the level of compaction between MPC and MPC:MVF regardless of culture condition (i.e., MM +/− AM or AM+) began to diverge from one another, with MPC:MVF groups retaining a higher degree of compaction/lower coverage area. Within the MPC and MPC:MVF groups, fluctuations occurred between MM +/− AM, although by day 18, AM conditions began to demonstrate a consistently less compaction/higher coverage area relative to the MM only group (Fig. 2B). This observation is consistent with measurements of the cross-sectional area, indicating a lesser degree of compaction in the AM conditions relative to the MM condition within each group and day 21 (Fig. 2C).

The CK activities of TE-SkMs containing both MPCs and MVFs were lower than those containing only MPCs regardless of the culture condition (i.e., MM +/− AM or AM+; Fig. 2D). The treatment of TE-SkMs containing MPCs with AM reduced the CK activity relative to treatment with MM only, whereas the treatment of TE-SkMs containing both MPCs and MVFs with AM increased the CK activity relative to treatment with MM only (Fig. 2D). Overall, the increased compaction of TE-SkMs containing both MVFs and MPCs is consistent with observations that microvessels positively increase aspects of myogenesis.[26] Although the measurements of the CK activity do not support this contention, an alternative possibility is that the increased degradation of the matrix due to matrix metalloproteinases provided by cells of the microvasculature[43] contributed to the increased compaction rate observed.

TE-SkM mechanical property assessment

TE-SkMs with MPCs alone or MPCs and MVFs treated with different culture conditions were subjected to tensile deformation to stress–strain profiles (Fig. 3A, B, respectively) to calculate ultimate tensile strength (UTS), elongation at failure, stiffness, and Young's modulus. The TE-SkMs containing both MPCs and MVFs groups cultured under MM conditions had the highest UTS (Fig. 3C) and Young's modulus (Fig. 3D). Regardless of culture condition, TE-SkMs with MPCs alone had an approximately threefold increase in stiffness relative to TE-SkMs containing both MPCs and MVFs (Fig. 3E). No significant differences in elongation at failure (Fig. 3F) were observed. While the inclusion of MVFs increased construct mechanical strength, the addition of adipogenesis diminished this improvement. A plausible explanation is that MVFs provide a source of myogenic factors that cause this improvement in the organization of the myogenic structures, whereas adipocytes tend to negate this augmentation. Regardless, the development of the current model containing these structures provides an opportunity to further investigate these phenomena.

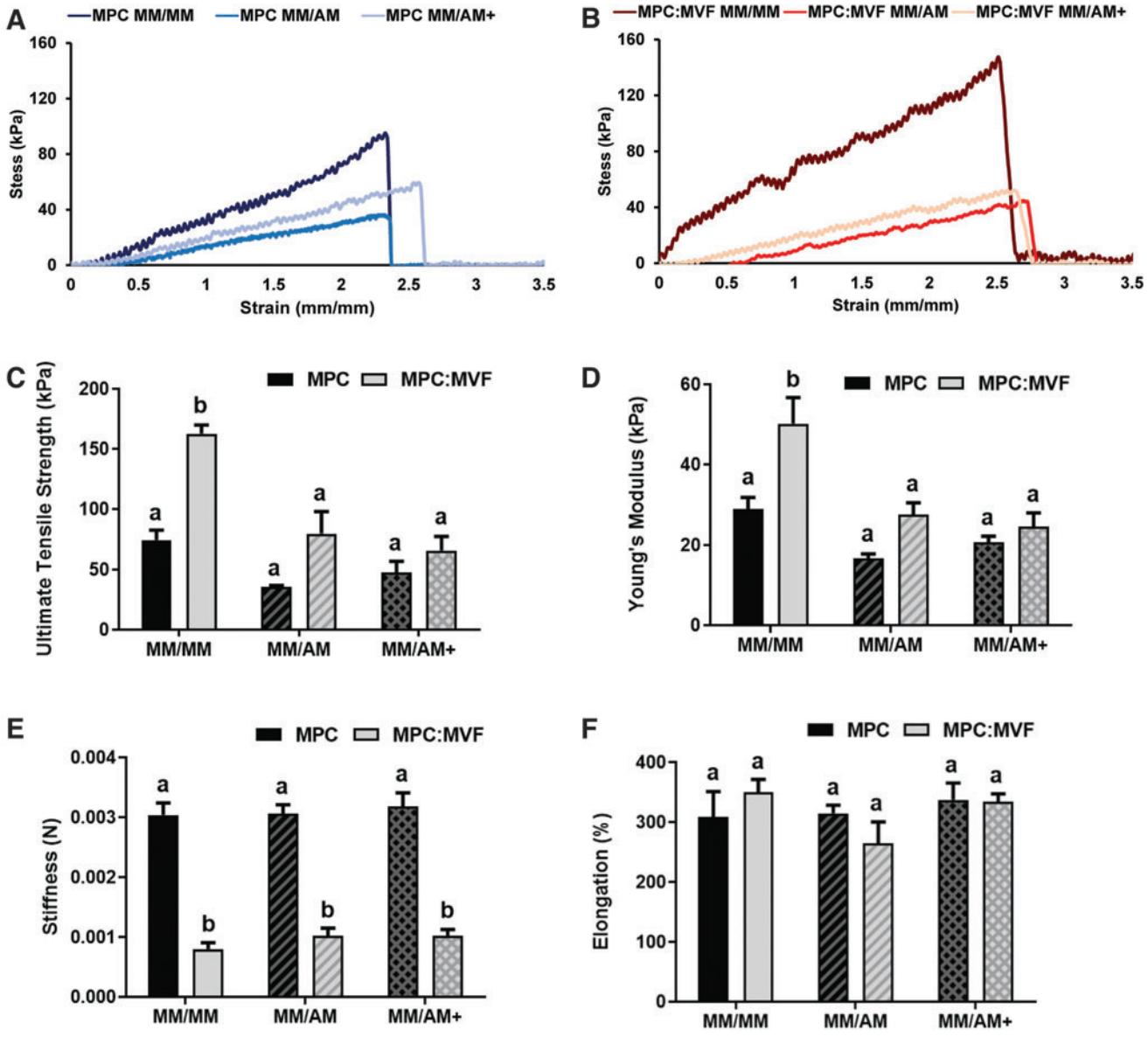

FIG. 3. Uniaxial tensile testing of TE-SkM. TE-SkM constructs containing MPC only or a combination of MPCs and MVFs (MPC:MVF) that were treated with MM only, or MM before two levels of adipogenic media (AM or AM+) ($n=4$ per group). Representative stress–strain profiles of TE-SkM containing MPCs **(A)** or MPCs and MVFs **(B)** treated with different media conditions were used for the calculation of **(C)** ultimate tensile strength (kPa), **(D)** Young's modulus (kPa), **(E)** stiffness (N), and **(F)** elongation at failure (%). Results are reported as mean ± standard error. *Bars displaying different letters* are statistically significant from each other ($p<0.05$). *Bars with the same letters* are not significantly different ($p>0.05$). Color images are available online.

Histological analysis of adipogenesis and angiogenesis in TE-SkM

No GS-Lectin I-positive structures (indicative of microvessels) were observed qualitatively (Fig. 4) or quantified (Fig. 5B, D) in TE-SkMs containing only MPCs. Regardless of culture condition, TE-SkMs containing both MPCs and MVFs were characterized by the presence of a high content of GS-Lectin I-positive structures (Fig. 4). The use of AM caused a change in the appearance of the microvessels, an effect that was most noticeable in the presence of AM+ (Fig. 4). Despite qualitative changes in vessel appearance with the use of AM or AM+, there were no differences in the percent area covered by microvessels (Lectin+ area) (Fig. 5B). The connectivity of the vascular structures was evaluated through the quantification of vessels using the object count attained when thresholding samples (Fig. 5D). Consistent with the observations of an altered appearance of the vessels with the use of AM+, there was an increase in the vessel count in this group indicative of a decreased vascular connectivity under this condition (Fig. 5D).

The use of AM or AM+ caused qualitative increases in lipid content indicative of an increase in the presence of adipocytes in both TE-SkMs containing MPCs alone or MPCs and MVFs compared with MM. The use of AM+ increased lipid content compared with AM for both MPC and MPC:MVF (Fig. 4). Consistent with these qualitative observations, the use of AM or AM+ resulted in an increase in the percent area covered by lipid (Fig. 5A) and lipid count (Fig. 5C) in both TE-SkMs containing MPCs alone or MPCs and MVFs compared with MM, and the use of AM+ increased lipid content compared with AM for both MPC and MPC:MVF. More specifically, an $\sim$1900% increase in lipid coverage area was observed with MM/AM+ and MM/AM in the MPC group, and an $\sim$200% increase in lipid coverage area was measured with MM/AM+ compared with MM/AM in the MPC:MVF group (Fig. 5A). Within the MPC only and MPC:MVF groups, $\sim$1000% and 74% increases in lipid count, respectively, were observed between MM/AM+ and MM/AM (Fig. 5C). The presence of MVFs increased the lipid content when both adipogenic conditions (AM or AM+) were used. TE-SkMs containing MPCs and MVFs had a higher percentage area covered by lipid (Fig. 5A) and lipid count (Fig. 5C) compared with TE-SkMs containing MPCs alone regardless of whether AM or AM+ was used. Collectively, the MPC:MVF group in MM/AM+ growth conditions had the most significant amount of adipocyte formation out of all groups tested.

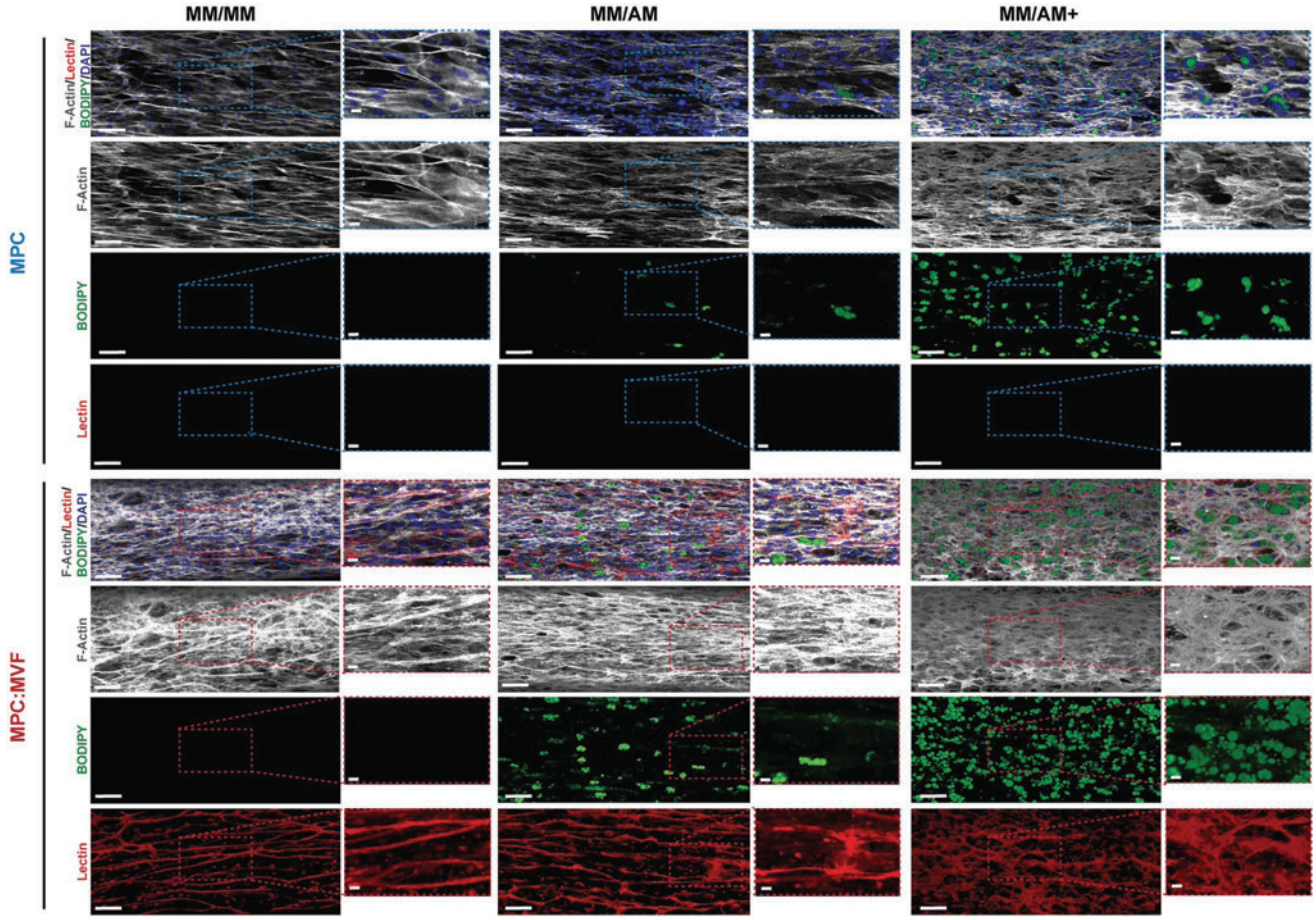

FIG. 4. Qualitative histological analysis of TE-SkM. Constructs containing MPC only or a combination of MPCs and MVFs (MPC:MVF) that were treated with MM only, or MM before two levels of adipogenic media (AM or AM+) were acquired after 21 days of treatment. TE-SkMs were stained with F-Actin (*white*) to visualize cytoskeletal components, DAPI (*Blue*) for visualization of nuclei, BODIPY (*green*) to identify the presence of lipid droplets, and GS Lectin I (*red*) for the visualization of microvessels. Scale bars = 200 μm. BODIPY, boron-dipyrromethene. Color images are available online.

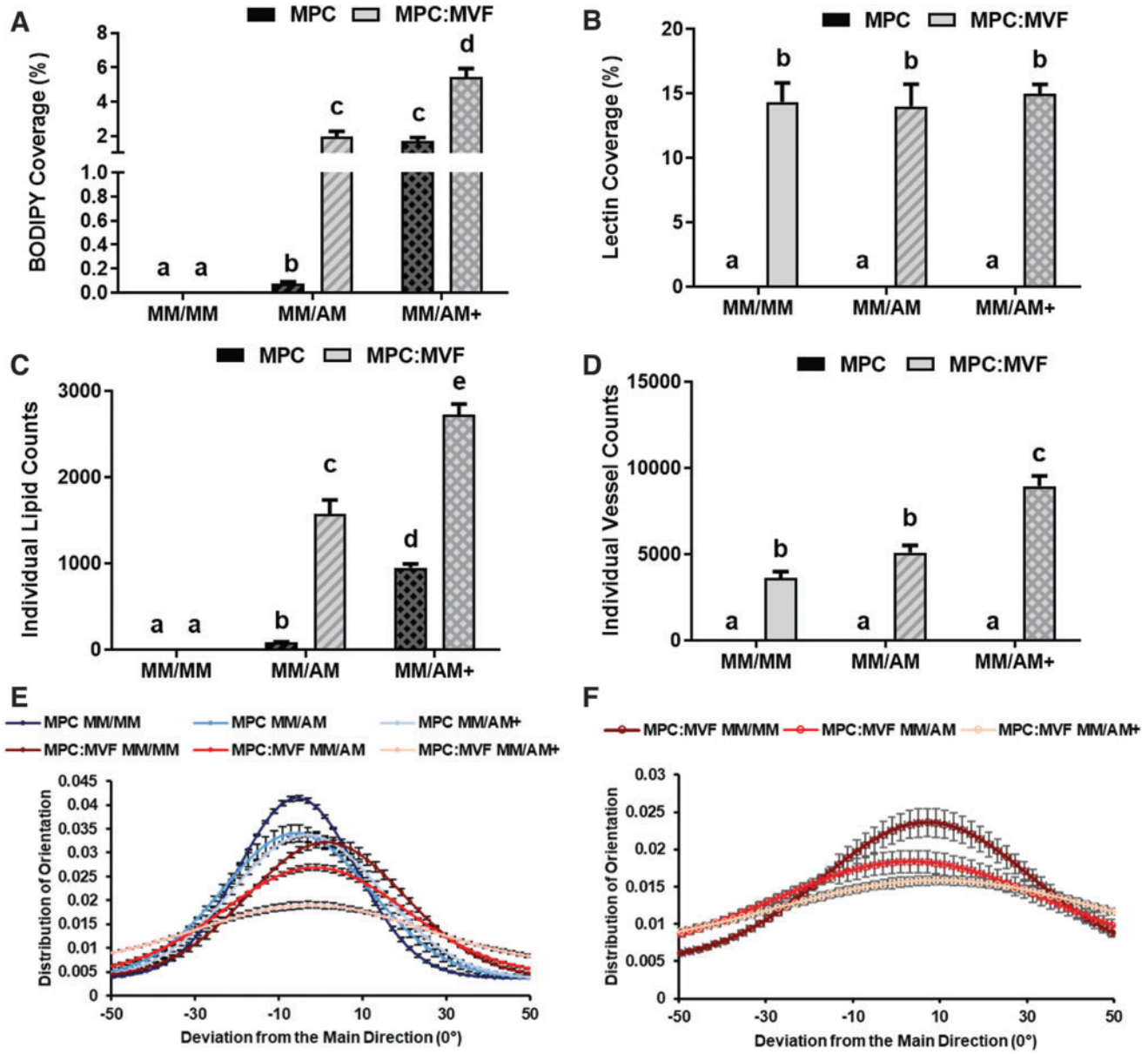

FIG. 5. Quantitative histological analysis of TE-SkM. Constructs containing MPC only or a combination of MPCs and MVFs (MPC:MVF) that were treated with MM only, or MM before two levels of adipogenic media (AM or AM+) ($n = 4$ per group). The quantification of mean fluorescence intensity of BODIPY staining **(A)**, quantification of mean fluorescence intensity of GS Lectin I staining **(B)**. The average object counts in imaged ROIs with BODIPY staining measuring interconnectivity of lipid droplets **(C)**, and average object counts in imaged ROIs with GS Lectin I staining measuring interconnectivity of vessel structures **(D)**, analysis of F-Actin alignment and orientation distribution within TE-SkMs **(E)**, analysis of GS Lectin I alignment and orientation distribution within TE-SkMs **(F)**, were measured using confocal images of TE-SkMs cultured for 21 days. Results are reported as mean ± standard error. *Bars displaying different letters* are statistically significant from each other ($p < 0.05$). *Bars with the same letters* are not significantly different ($p > 0.05$). ROIs, regions of interest. Color images are available online.

To investigate the spatial effect of microvessels and adipocytes on myogenic structure alignment and orientation within TE-SkMs, F-actin fluorescence staining was analyzed (Fig. 5E); samples that were more aligned displayed a narrow distribution plot, suggesting a high degree of cell organization. Generally speaking, MPC only groups had a greater degree of alignment than the MPC:MVF groups; however, with both groups, a reduction in alignment occurred in the context of AM (MM/AM and MM/AM+). The GS-Lectin I fluorescence staining within the MPC:MVF groups was also analyzed to specifically determine the effect of lipids on vascular organization (Fig. 5F). Similar to that observed where AM disrupted myogenic structure alignment, AM reduced the alignment of vascular structures (Fig. 5F). Notably, this effect was most pronounced in the context of AM+, where the highest level of lipid content was observed. Overall, taken together with the robust changes in the overall quantity of lipid and microvessels, the changes in

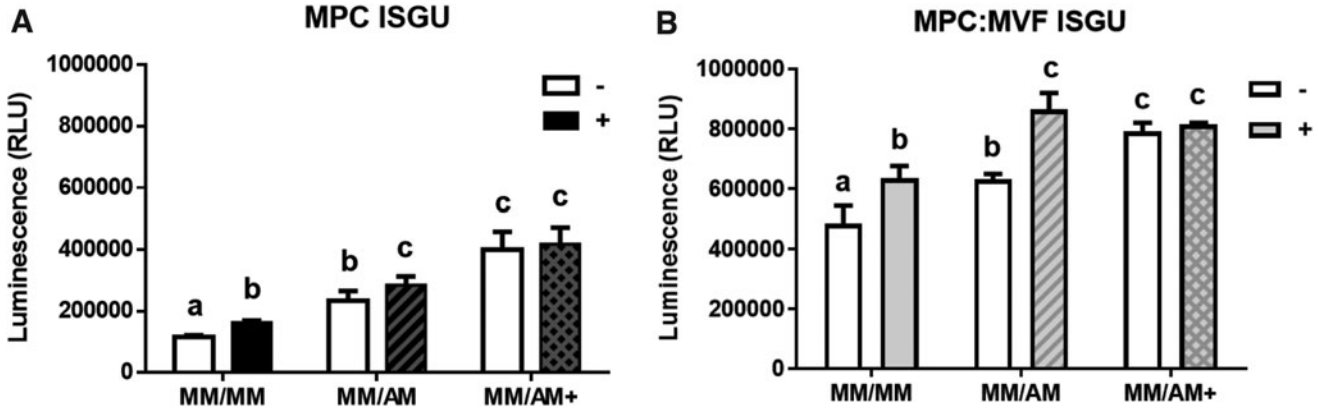

FIG. 6. Metabolic function characterization of TE-SkM. Constructs containing MPC only or a combination of MPCs and MVFs (MPC:MVF) that were treated with MM only, or MM before two levels of adipogenic media (AM or AM+) ($n=6$ per group). Average luminescence measurements indicative of 2DG6P uptake (RLU), an index of ISGU, in TE-SkMs in the MPC **(A)** and MPC:MVF **(B)** groups cultured under the different media conditions for 21 days, before (*open bars*) and after (*shaded bars*) insulin stimulation. Results are reported as mean ± standard error. *Bars displaying different letters* are statistically significant from each other ($p<0.05$). *Bars with the same letters* are not significantly different ($p>0.05$). 2DG6P, 2-deoxyglucose-6-phosphate; ISGU, insulin-stimulated glucose uptake; RLU, relative light units.

the alignment of the structures within the TE-SkMs point to a significant alteration in the structural integrity, an observation that is supported by alterations in the mechanical characterization (Fig. 3C, D). This proposition is supported by previous findings where increased lipid in engineered skeletal muscle reduced electrically induced functional outcomes.[44]

TE-SkM metabolic assessment

Overall, TE-SkMs containing both MPCs and MVFs had a higher insulin-stimulated glucose uptake (ISGU) activity compared with TE-SkMs containing MPC only (Fig. 6A, B). In TE-SkMs containing either MPCs or MPCs and MVFs and treated with either MM/MM or MM/AM conditions, a physiological response of glucose uptake was exhibited as demonstrated by a significant increase in 2DG6P uptake in response to insulin treatment; however, when TE-SkMs were cultured in MM/AM+, no significant increase in ISGU was observed (Fig. 6A, B). Overall, the amount of glucose internalized was higher in groups exposed to AM/AM+ conditions compared with constructs in MM/MM culture, irrespective of MPC or MPC:MVF seeding. Adipocytes increase glucose uptake in response to insulin; therefore, the increase in basal ISGU in constructs with and without MVFs with adipogenic induction is logical.[45,46] The reduced responsiveness of the TE-SkMs to insulin at the highest levels of adipogenesis is intriguing and leads to the speculation that higher level of adipogenesis causes a transition to a more pathological state.

qPCR analysis of TE-SkMs

Generally speaking, there were no major trends signifying differences in muscle marker expression, though intermittent increases in muscle marker expression are seen while in adipogenic conditions (Fig. 7A–C). Specifically, the two early myogenic markers, *MyoD* and *Myogenin*, are increased in MPC in MM/AM culture, whereas the late myogenic marker, *MHC*, is upregulated in MPC:MVF in MM/AM+ conditions. Analysis of key adipogenic markers peroxisome *proliferator-activated receptor-gamma (PPARγ)*, *adiponectin*, and fatty-acid synthase (*FAS*) confirmed the formation of adipocytes in cultures of MM/AM and MM/AM+ (Fig. 7D–F), showing similar trends among all genes. *PPARγ* fold expression in TE-SkMs containing MPCs was significantly higher in adipogenic differentiation conditions with an ~1000-fold increase in both MM/AM and MM/AM+. In TE-SkMs containing MPCs and MVFs, an ~1750-fold increase was observed in MM/AM culture conditions and ~6000-fold increase in MM/AM+ for *PPARγ*. The *adiponectin* fold expression within TE-SkMs containing MPCs increased ~1000-fold in both MM/AM and MM/AM+ conditions. Within TE-SkMs containing MPCs and

FIG. 7. qPCR analysis of myogenic, adipogenic, and angiogenic markers in TE-SkM. Constructs containing MPC only or a combination of MPCs and MVFs (MPC:MVF) that were treated with MM only, or MM before two levels of adipogenic media (AM or AM+) ($n=4$ per group). The different bars represent: fold expression of **(A)** MyoD, **(B)** MYOG, and **(C)** MHC, **(D)** *PPARγ*, **(E)** adiponectin, **(F)** Fas cell surface death receptor (*FAS*), **(G)** an early angiogenic marker (FLK1), **(H)** a later marker for angiogenesis, ANGPT1, and **(I)** VEGF. Results were normalized based on their respective MM/MM control group. Results are reported as mean ± standard error ($n=4$). *Bars displaying different letters* are statistically significant from each other ($p<0.05$). *Bars with the same letters* are not significantly different ($p>0.05$). ANGPT1, angiopoietin 1; FLK1, fetal liver kinase-1; MHC, myosin heavy chain; MyoD, myoblast determination protein 1; MYOG, myogenin; *PPARγ*, peroxisome proliferator-activated receptor-gamma; VEGF, vascular endothelial growth factor.

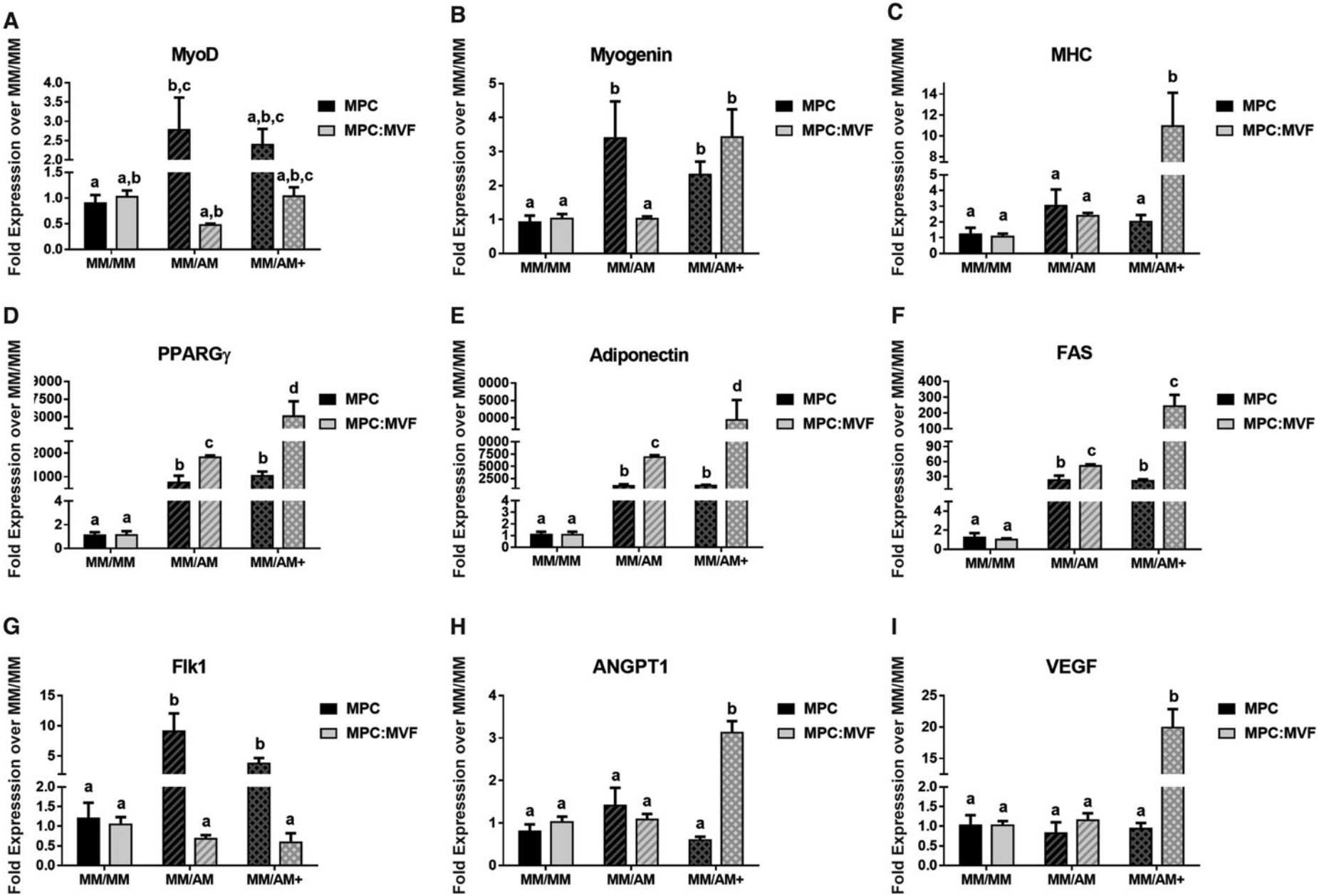
A
MyoD
Fold Expression over MM/MM
MPC
MPC:MVF
MM/MM
MM/AM
MM/AM+
B
Myogenin
C
MHC
D
PPARGγ
E
Adiponectin
F
FAS
G
Flk1
H
ANGPT1
I
VEGF

MVFs, an ~6000-fold increase was observed in MM/AM and ~3000-fold increase in MM/AM+ for *adiponectin*. For TE-SkMs containing MPCs, *FAS* expression increased ~20-fold in both MM/AM and MM/AM+ conditions. For TE-SkMs containing MPCs and MVFs, an *FAS* expression increased ~45-fold in MM/AM and ~250-fold in MM/AM+. The only major difference observed in the analysis of angiogenic markers fetal liver kinase-1 (*FLK1*), *angiopoietin 1 (ANGPT1)*, and *vascular endothelial growth factor* (*VEGF*; Fig. 7G–I) was within the TE-SkMs containing only MPCs where an upregulation of *FLK1* in the MM/AM condition was observed. Within TE-SkMs containing MPCs and MVFs, an upregulation of *ANGPT1* and *VEGF* was observed in the MM/AM+ condition.

Discussion

The engineering of skeletal muscle systems with directionality and alignment that represent the organization of skeletal muscle as seen *in vivo* has largely been considered a promising approach for improving tissue regeneration, in cases such as volumetric muscle loss, and is also regarded as an effective means to create a high-throughput, patient-derived biomimetic system for disease modeling.[31,47,48] Accordingly, skeletal muscle systems have been developed to incorporate the interaction of cells/structures that are present within skeletal muscle to develop models that more accurately represent skeletal muscle's multicellular composition and metabolic function; examples of cells/structures that have been used to improve engineered skeletal muscle include microvessels, fibroblasts, macrophages, and neurons.[1–5] In addition to improving the utility of engineered skeletal muscle systems to support research into skeletal muscle phenomena, these improvements also support the development of improved drug-screening platforms. With this objective in mind, in the current study, a TE-SkM model was developed through the formation of a system containing muscle cells, adipocytes, and microvessels; this system more accurately portrays the skeletal muscle environment, especially where the number of adipocytes is increased. This objective was accomplished through the use of MPCs with or without MVFs as the cell source, and an appropriately timed application of AM to allow time for angiogenesis to develop while also providing the stimulus for the adipogenic differentiation of cells within the constructs.

The inclusion of a microvasculature is perhaps the most obvious benefit to the TE-SkM developed in the current study. Skeletal muscle is highly vascularized to meet the high energetic demand for muscle activity. The smallest contractile unit of a skeletal muscle, the muscle fiber or myofiber, is perfused by microvessels that are parallel to it. Consequently, endothelial capillaries and muscle fibers lie in proximity to one another and therefore are subjected to continuous cross talk. This interaction is worthy of investigation in the context of diseases such as diabetes, where reduced capillarization puts diabetic patients at a greater risk for peripheral arterial disease, and eventually, critical limb ischemia compared with those without diabetes.[17,49,50] MVFs impart several advantages to create vascularized engineered tissues and have been used previously for this purpose.[33–38] In the current study, the use of MVFs was an effective means for creating a highly vascularized TE-SkM as demonstrated by a persistent and robust microvascular network (Figs. 4 and 5B, D). Histologically (Fig. 4), we are able to appreciate a high degree of vessel formation on all groups in which MVFs are present, although notably, the integrity of the vascular structure diminishes as fat formation is increased. Quantification of vessel formation through lectin showed no significant difference in the total amount of vessel formation (Fig. 5B). However, it was shown that as fat formation increases between MM/AM and MM/AM+ in MPC:MVF groups, there was a decrease in the alignment of vascular structures (Fig. 5F). Additionally, there was a significant decline in the interconnectivity of vessels formed, revealed through the increase in object counts of lectin in ROIs of MPC:MVF in MM/AM+, where the highest amount of fat formed was observed (Fig. 5D). To create a more advanced system with an increased multicellularity, the microvessels were allowed to develop before the exposure to adipogenic differentiation conditions to increase the adipocyte content within them, thus creating a vascularized TE-SkM with increased adipocyte content. When taking into consideration the increased IMAT in diabetic patients,[10,16,17] this is a platform to study the interaction among muscle cells, the microvasculature, and adipocytes in the progression of disease. It is also worth mentioning that the model developed herein has potential applications for the study of other skeletal muscle pathologies as well, given the presence of IMAT in the context of other diseases/conditions.[11–13,51,52]

It is important to point out that it was intended that the system be relatively straightforward, without requiring a multitude of cellular inputs to be successful. To this end, two cellular components (MPCs and MVFs) were used, and it was from both of these sources that myogenesis, angiogenesis, and adipogenesis were achieved. Previous research demonstrated a favorable interaction between MPCs and MVFs, in particular, that MPCs secrete factors that promote angiogenesis,[53,54] a feature of the system that supports the maintenance of a persistent microvasculature. The goal of introducing adipocytes into the system while maintaining a microvasculature is not as straightforward, but when taking into consideration the adipogenic potential of both MPCs and resident stem cells within the MVFs, the rationale for their inclusion, and the lack of a need for an additional cellular input (i.e., multipotent stem cells), becomes more apparent.[34,39,41,55]

The timing of adipogenic induction is a critical factor to consider. Previous work established that the timing of adipogenic induction is critical to maintaining the balance between angiogenesis, myogenesis, and adipogenesis.[34,41] Specifically, direct exposure (i.e., without previous myogenesis or angiogenesis) to adipogenic differentiation can increase the adipogenic potential of these cells, but especially with MVFs, this may come at the expense of vascular development. Since the goal was to have all cellular components coexisting in parallel, a ''pre-sprouting'' phase was included for all groups, meaning that TE-SkMs were cultured in MM conditions for 7 days, thus allowing sufficient time for vessel growth before stimulation of adipogenesis.

Several observations support the contention that the augmentation of the vascularized constructs with adipocytes had an impact on the structural and functional characteristics of

the engineered tissues and provide the impetus for future study. Compaction, cross-sectional area, and CK activity were evaluated to gain insight into the effect of TE-SkM maturation[56–59] (Fig. 2A–D). Specifically, compaction, which measures changes to the gel surface area over time, is correlated with the protein and cell content of constructs, as well as TE-SkM architecture, function, maturity, and strength.[56–58]

This is similar to what can be said when measuring endpoint cross-sectional area. Additionally, increasing levels of the CK activity have been presented to be a sign of muscle maturation.[59] The smaller coverage area and cross-sectional area when MVFs were combined with MPCs indicate that the vascularization of the engineered muscle constructs had a positive effect on maturation (Fig. 2A–C). The presence of adipocytes in the vascularized constructs was robust when taking into consideration the large increase in BODIPY (used as a surrogate for adipocytes) staining (Figs. 4 and 5). This modification generally had a negative effect on the maturation and organization of the engineered constructs, especially in constructs containing MVFs. Correlating histological findings (Figs. 4 and 5) and data presented in Figure 2, we specifically observe that more disorganized/less aligned structures (groups with AM) ended up having less compaction/higher coverage area, indicative of a less maturation; we can also pinpoint the source of this disruption being the presence of adipocytes, as demonstrated through BODIPY staining.

Although a more heterogeneous model may be expected to have a higher level of disorganization, it is also worth noting that skeletal muscle is a highly organized tissue, thus alignment of F-actin filaments (Fig. 5E) and vascular structures (Fig. 5F) was looked at, and correlations were seen to the level compaction/maturation observed (Fig. 2), where increasing adipocyte content disrupted alignment and also decreased compaction/maturation. Furthermore, the addition of adipogenic induction media to constructs containing microvessels caused a reduction in compaction over time and an increased cross-sectional area; however, it was also accompanied by an increase in the CK activity (Fig. 2A–D). This discrepancy between compaction and CK activity cannot completely be explained by changes in myogenic gene expression; only the adipogenic induction conditions that caused the highest adipocyte content (AM+) increased *myogenin* and *myosin heavy chain* gene expression (Fig. 7A–C). Seemingly conflicting results of muscle maturity between compaction, CK activity, and myogenic gene expression may be partially explained by the presence of hormones in the AM such as T3, which has been found to promote the activation of the *MyoD* gene in myogenic cell lines.[60] Given their diverse cell populations, when comparing MPC versus MPC:MVF groups, CK results should be taken as non-absolute, even though there is seemingly a drop in maturation with MVFs. The compaction differences could potentially be explained by the significant increases in lipid formation, which may have caused a hindrance in compaction.

To gain further insight into the effect of augmenting constructs with adipocytes, both those containing MVFs and those that did not, uniaxial tensile mechanical characterization of TE-SkM was used as a means of evaluating TE-SkM mechanical integrity.[61–63] Examining the stress–strain profiles alone (Fig. 3A, B), all groups showed viscoelastic curves typically seen in soft biologic tissue,[64] and all the constructs displayed Young's modulus that fall within the range between $\sim$12 and 2800 kPa, which is characteristic of skeletal muscle.[65,66] The salient findings among the mechanical parameters evaluated are that: (1) in the absence of adipogenesis (MM/MM condition), the inclusion of MVFs increased the mechanical strength of the constructs and (2) augmentation of adipogenesis in constructs containing MVFs diminished this improvement in mechanical integrity (Fig. 3C, D). Recent work where the exposure of engineered skeletal muscle to fatty acids resulted in increased lipid accumulation, and reductions in tetanic and single twitch force concomitant with altered insulin signaling.[44] Although the tensile mechanical characterization of the TE-SkM in the current study implies changes in electrically invoked muscle contraction may occur, measurements of twitch and tetanus would have provided a more comprehensive understanding of the functional implications of the presence of adipocytes in vascularized TE-SkM, and the lack of these measurements limits a more comprehensive understanding of the model.

Nonetheless, the altered mechanical integrity observed is in agreement with the finding that increased adipocyte content caused changes in the alignment of myogenic and vascular structures, an effect that was visualized qualitatively (Fig. 4), and quantified in both nonvascularized (MPC) and vascularized (MPC:MVF) constructs (Fig. 5E). These results, as well as an alteration in the alignment of microvessels in vascularized constructs (Fig. 5F), support the contention that adipocytes alter the structural integrity of engineered constructs toward a less organized form and potentially reduces their integrity. Collectively, the parallelism in the findings from compaction (Fig. 2A–C), mechanical analyses (Fig. 3C, D), cell and vessel alignment (Figs. 4 and 5E, F) suggests that an increase in adipocyte content interferes with the structural integrity of vascularized skeletal muscle. This is especially interesting to consider when taken together with the findings that the presence of intermuscular adipose tissue had a direct effect on skeletal muscle function *in vivo*, where a vasculature was present.[67]

In addition to the modifications imparted to TE-SkM by microvessels and adipocytes, the effect of these parameters on metabolic properties was evaluated. In agreement with other investigations, constructs made without the modification of MVFs or adipocytes exhibited an increase in glucose uptake in response to insulin[40,68] (Fig. 6A). The addition of MVFs resulted in a similar response, that is, TE-SkMs containing MVFs exhibited an increase in glucose uptake in response to insulin (Fig. 6B). The induction of adipogenesis resulted in an increase in basal ISGU in both constructs with and without MVFs, which is in agreement and reflective of the increase in adipocyte content since adipocytes also increase glucose uptake in response to insulin.[45,46] Two different adipogenic induction conditions were used to determine if the content of adipocytes could be controlled, specifically, although both medias contained insulin, forskolin, and dexamethasone, the ''AM+'' media was supplemented with Rosi and T3. This more potent adipogenic induction media significantly increased adipocyte quantity that was seen visually (Fig. 4) and was measured quantitatively (Fig. 5A, C). In agreement with this increase in

adipocyte content, the basal level of glucose uptake in response to insulin was increased, which suggests that additional adipocytes had an effect on the metabolism of the TE-SkMs; however, the glucose uptake in response to insulin was no longer seen. Through speculation, we can attribute this response to the TE-SkM construct depicting a ''diabetic-like'' response where insulin sensitivity is altered potentially due to the large degree of fat present in the environment. This conclusion is indicative that fat formation alone in this model was enough to warrant a biomimetic disease response of a reduction in ISGU, and the introduction of a diseased cell source was not needed to replicate the pathology.

Conclusions

In summary, these findings represent the development of a comprehensive tri-TE-SkM model with the incorporation of MPCs, adipocytes, and microvessels. The simple approach that utilized MPCs and MVFs to develop a vascularized skeletal muscle model with adipocytes more closely mimics the structural and functional characteristics seen *in vivo*, and this may be especially useful for modeling skeletal muscle diseases. Future research will focus on using this model as a tool for drug and treatment testing to counteract metabolic diseases and build on its capabilities by incorporating additional factors, such as disease-derived cell sources.

Disclosure Statement

No competing financial interests exist.

Funding Information

This work was supported, in part, by the National Institutes of Health (Grant Nos. SC1DK122578 and 5RO1EB020604), Veterans Administration (Grant No. 5 I01 BX000418-06), the University of Texas System Science and Technology Acquisition and Retention Program, the University of Texas Department of Biomedical Engineering and Chemical Engineering, and the UTSA RISE Research Training Program (Grant No. NIH GM060655).

Supplementary Material

Supplementary Table S1

References

1. Osaki, T., Sivathanu, V., and Kamm, R.D. Crosstalk between developing vasculature and optogenetically engineered skeletal muscle improves muscle contraction and angiogenesis. Biomaterials **156,** 65, 2018.
2. Levenberg, S., Rouwkema, J., Macdonald, M., *et al.* Engineering vascularized skeletal muscle tissue. Nat Biotechnol **23,** 879, 2005.
3. Kalman, B., Monge, C., Bigot, A., *et al.* Engineering human 3D micromuscles with co-culture of fibroblasts and myoblasts. Comput Methods Biomech Biomed Engin **18 Suppl 1,** 1960, 2015.
4. Osaki, T., Uzel, S.G.M., and Kamm, R.D. Microphysiological 3D model of amyotrophic lateral sclerosis (ALS) from human iPS-derived muscle cells and optogenetic motor neurons. Sci Adv **4,** eaat5847, 2018.
5. Juhas, M., Abutaleb, N., Wang, J.T., *et al.* Incorporation of macrophages into engineered skeletal muscle enables enhanced muscle regeneration. Nat Biomed Eng **2,** 942, 2018.
6. Maffioletti, S.M., Sarcar, S., Henderson, A.B.H., *et al.* Three-dimensional human iPSC-derived artificial skeletal muscles model muscular dystrophies and enable multilineage tissue engineering. Cell Rep **23,** 899, 2018.
7. Gallagher, D., Kuznia, P., Heshka, S., *et al.* Adipose tissue in muscle: a novel depot similar in size to visceral adipose tissue. Am J Clin Nutr **81,** 903, 2005.
8. Hilton, T.N., Tuttle, L.J., Bohnert, K.L., Mueller, M.J., and Sinacore, D.R. Excessive adipose tissue infiltration in skeletal muscle in individuals with obesity, diabetes mellitus, and peripheral neuropathy: association with performance and function. Phys Ther **88,** 1336, 2008.
9. Marcus, R.L., Addison, O., Kidde, J.P., Dibble, L.E., and Lastayo, P.C. Skeletal muscle fat infiltration: impact of age, inactivity, and exercise. J Nutr Health Aging **14,** 362, 2010.
10. Goodpaster, B.H., Thaete, F.L., and Kelley, D.E. Thigh adipose tissue distribution is associated with insulin resistance in obesity and in type 2 diabetes mellitus. Am J Clin Nutr **71,** 885, 2000.
11. Goodpaster, B.H., Chomentowski, P., Ward, B.K., *et al.* Effects of physical activity on strength and skeletal muscle fat infiltration in older adults: a randomized controlled trial. J Appl Physiol **105,** 1498, 2008.
12. Goodpaster, B.H., Carlson, C.L., Visser, M., *et al.* Attenuation of skeletal muscle and strength in the elderly: the Health ABC Study. J Appl Physiol **90,** 2157, 2001.
13. Gaeta, M., Messina, S., Mileto, A., *et al.* Muscle fat-fraction and mapping in Duchenne muscular dystrophy: evaluation of disease distribution and correlation with clinical assessments. Preliminary experience. Skeletal Radiol **41,** 955, 2012.
14. Kovalik, J.P., Slentz, D., Stevens, R.D., *et al.* Metabolic remodeling of human skeletal myocytes by cocultured adipocytes depends on the lipolytic state of the system, Diabetes **60,** 1882, 2011.
15. Dietze, D., Koenen, M., Röhrig, K., *et al.* Impairment of insulin signaling in human skeletal muscle cells by coculture with human adipocytes. Diabetes **51,** 2369, 2002.
16. Lillioja, S., Young, A.A., Culter, C.L., *et al.* Skeletal muscle capillary density and fiber type are possible determinants of in vivo insulin resistance in man. J Clin Invest **80,** 415, 1987.
17. Marin, P., Andersson, B., Krotkiewski, M., and Bjorntorp, P. Muscle fiber composition and capillary density in women and men with NIDDM. Diabetes Care **17,** 382, 1994.
18. Spencer, M., Unal, R., Zhu, B., *et al.* Adipose tissue extracellular matrix and vascular abnormalities in obesity and insulin resistance. J Clin Endocrinol Metab **96,** E1990, 2011.
19. Aswad, H., Forterre, A., Wiklander, O.P., *et al.* Exosomes participate in the alteration of muscle homeostasis during lipid-induced insulin resistance in mice. Diabetologia **57,** 2155, 2014.
20. Webster, C., and Blau, H.M. Accelerated age-related decline in replicative life-span of Duchenne muscular dystrophy myoblasts: implications for cell and gene therapy. Somat Cell Mol Genet **16,** 557, 1990.
21. Renault, V., Thornell, L.E., Eriksson, P.O., Butler-Browne, G., and Mouly, V. Regenerative potential of human skeletal muscle during aging. Aging Cell **1,** 132, 2002.

22. Nguyen, F., Guigand, L., Goubault-Leroux, I., Wyers, M., and Cherel, Y. Microvessel density in muscles of dogs with golden retriever muscular dystrophy. Neuromuscul Disord **15,** 154, 2005.
23. Ryan, N.A., Zwetsloot, K.A., Westerkamp, L.M., *et al.* Lower skeletal muscle capillarization and VEGF expression in aged vs. young men. J Appl Physiol **100,** 178, 2006.
24. Rhoads, R.P., Flann, K.L., Cardinal, T.R., *et al.* Satellite cells isolated from aged or dystrophic muscle exhibit a reduced capacity to promote angiogenesis in vitro. Biochem Biophys Res Commun **440,** 399, 2013.
25. Amir Levy, Y., Ciaraldi, T.P., Mudaliar, S.R., Phillips, S.A., and Henry, R.R. Excessive secretion of IL-8 by skeletal muscle in type 2 diabetes impairs tube growth: potential role of PI3K and the Tie2 receptor. Am J Physiol Endocrinol Metab **309,** E22, 2015.
26. Christov, C., Chrétien, F., Abou-Khalil, R., *et al.* Muscle satellite cells and endothelial cells: close neighbors and privileged partners. Mol Biol Cell **18,** 1397, 2007.
27. Verma, M., Asakura, Y., Murakonda BSR, *et al.* Muscle satellite cell cross-talk with a vascular niche maintains quiescence via VEGF and Notch signaling. Cell Stem Cell **23,** 530, 2018.
28. Pellegrinelli, V., Rouault, C., Rodriguez-Cuenca, S., *et al.* Human adipocytes induce inflammation and atrophy in muscle cells during obesity. Diabetes **64,** 3121, 2015.
29. Takegahara, Y., Yamanouchi, K., Nakamura, K., Nakano, S., and Nishihara, M. Myotube formation is affected by adipogenic lineage cells in a cell-to-cell contact-independent manner. Exp Cell Res **324,** 105, 2014.
30. Gholobova, D., Terrie, L., Gerard, M., Declercq, H., and Thorrez, L. Vascularization of tissue-engineered skeletal muscle constructs. Biomaterials **235,** 119708, 2020.
31. Gilbert-Honick, J., and Grayson, W. Vascularized and innervated skeletal muscle tissue engineering. Adv Healthc Mater **9,** e1900626, 2020.
32. Hoying, J.B., Boswell, C.A., and Williams, S.K. Angiogenic potential of microvessel fragments established in three-dimensional collagen gels. In Vitro Cell Dev Biol Anim **32,** 409, 1996.
33. Shepherd, B.R., Chen, H.Y., Smith, C.M., *et al.* Rapid perfusion and network remodeling in a microvascular construct after implantation. Arterioscler Thromb Vasc Biol **24,** 898, 2004.
34. Acosta, F., Stojkova, K., Brey, E.M., and Rathbone, C. A straightforward approach to engineer vascularized adipose tissue using microvascular fragments. Tissue Eng Part A **26,** 905, 2020.
35. Pilia, M., McDaniel, J.S., Guda, T., *et al.* Transplantation and perfusion of microvascular fragments in a rodent model of volumetric muscle loss injury. Eur Cell Mater **28,** 11, 2014; discussion 23–24.
36. Laschke, M.W., and Menger, M.D. Adipose tissue-derived microvascular fragments: natural vascularization units for regenerative medicine. Trends Biotechnol **33,** 442, 2015.
37. Frueh, F.S., Spater, T., Lindenblatt, N., *et al.* Adipose tissue-derived microvascular fragments improve vascularization, lymphangiogenesis, and integration of dermal skin substitutes. J Invest Dermatol **137,** 217, 2017.
38. Laschke, M.W., Kleer, S., Scheuer, C., *et al.* Vascularisation of porous scaffolds is improved by incorporation of adipose tissue-derived microvascular fragments. Eur Cell Mater **24,** 266, 2012.
39. McDaniel, J.S., Pilia, M., Ward, C.L., Pollot, B.E., and Rathbone, C.R. Characterization and multilineage potential of cells derived from isolated microvascular fragments. J Surg Res **192,** 214, 2014.
40. Acosta, F.M., Jia, U.A., Stojkova, K., *et al.* Diabetic conditions confer metabolic and structural modifications to tissue-engineered skeletal muscle. Tissue Eng Part A **27,** 549, 2021.
41. Acosta, F.M., Jia, U.A., Stojkova, K., *et al.* Divergent effects of myogenic differentiation and diabetes on the capacity for muscle precursor cell adipogenic differentiation in a fibrin matrix. Biochem Biophys Res Commun **526,** 21, 2020.
42. Livak, K.J., and Schmittgen, T.D. Analysis of relative gene expression data using real-time quantitative PCR and the 2(-Delta Delta C(T)) method. Methods **25,** 402, 2001.
43. Haas, T.L., Davis, S.J., and Madri, J.A. Three-dimensional type I collagen lattices induce coordinate expression of matrix metalloproteinases MT1-MMP and MMP-2 in microvascular endothelial cells. J Biol Chem **273,** 3604, 1998.
44. Turner, M.C., Rimington, R.P., Martin NRW, *et al.* Physiological and pathophysiological concentrations of fatty acids induce lipid droplet accumulation and impair functional performance of tissue engineered skeletal muscle. J Cell Physiol 2021. DOI: 10.1002/jcp.30365.
45. Shih, K.C., Kwok, C.F., and Ho, L.T. Combined use of insulin and endothelin-1 causes decrease of protein expression of beta-subunit of insulin receptor, insulin receptor substrate-1, and insulin-stimulated glucose uptake in rat adipocytes. J Cell Biochem **78,** 231, 2000.
46. White, M.F., and Kahn, C.R. The insulin signaling system. J Biol Chem **269,** 1, 1994.
47. Wang, J., Khodabukus, A., Rao, L., *et al.* Engineered skeletal muscles for disease modeling and drug discovery. Biomaterials **221,** 119416, 2019.
48. Vandenburgh, H. High-content drug screening with engineered musculoskeletal tissues. Tissue Eng Part B Rev **16,** 55, 2010.
49. Beckman, J.A., Creager, M.A., and Libby, P. Diabetes and atherosclerosis: epidemiology, pathophysiology, and management. JAMA **287,** 2570, 2002.
50. Ouriel, K. Peripheral arterial disease. Lancet **358,** 1257, 2001.
51. Sachs, S., Zarini, S., Kahn, D.E., *et al.* Intermuscular adipose tissue directly modulates skeletal muscle insulin sensitivity in humans. Am J Physiol Endocrinol Metabol **316,** E866, 2019.
52. Yang, Y., Ding, L., Zou, X., *et al.* Visceral adiposity and high intramuscular fat deposition independently predict critical illness in patients with SARS-CoV-2. Obesity (Silver Spring) **28,** 2040, 2020.
53. Rhoads, R.P., Johnson, R.M., Rathbone, C.R., *et al.* Satellite cell-mediated angiogenesis in vitro coincides with a functional hypoxia-inducible factor pathway. Am J Physiol Cell Physiol **296,** C1321, 2009.
54. Li, M.T., Ruehle, M.A., Stevens, H.Y., *et al.* *Skeletal myoblast-seeded vascularized tissue scaffolds in the treatment of a large volumetric muscle defect in the rat biceps femoris muscle. Tissue Eng Part A **23,** 989, 2017.
55. Scarda, A., Franzin, C., Milan, G., *et al.* Increased adipogenic conversion of muscle satellite cells in obese Zucker rats. Int J Obes (Lond) **34,** 1319, 2010.

56. Rowe, S.L., and Stegemann, J.P. Interpenetrating collagen-fibrin composite matrices with varying protein contents and ratios. Biomacromolecules **7,** 2942, 2006.
57. Shi, Y., Rittman, L., and Vesely, I. Novel geometries for tissue-engineered tendonous collagen constructs. Tissue Eng **12,** 2601, 2006.
58. Bian, W., and Bursac, N. Engineered skeletal muscle tissue networks with controllable architecture. Biomaterials **30,** 1401, 2009.
59. Ziter, F.A. Creatine kinase in developing skeletal and cardiac muscle of the rat. Exp Neurol **43,** 539, 1974.
60. Muscat, G.E., Mynett-Johnson, L., Dowhan, D., Downes, M., and Griggs, R. Activation of myoD gene transcription by 3,5,3'-triiodo-L-thyronine: a direct role for the thyroid hormone and retinoid X receptors. Nucleic Acids Res **22,** 583, 1994.
61. Ladd, M.R., Lee, S.J., Stitzel, J.D., Atala, A., and Yoo, J.J. Co-electrospun dual scaffolding system with potential for muscle-tendon junction tissue engineering. Biomaterials **32,** 1549, 2011.
62. Li, W.J., Mauck, R.L., Cooper, J.A., Yuan, X., and Tuan, R.S. Engineering controllable anisotropy in electrospun biodegradable nanofibrous scaffolds for musculoskeletal tissue engineering. J Biomech **40,** 1686, 2007.
63. Tiburcy, M., Markov, A., Kraemer, L.K., *et al.* Regeneration competent satellite cell niches in rat engineered skeletal muscle. FASEB Bioadv **1,** 731, 2019.
64. Gaur, P., Chawla, A., Verma, K., *et al.* Characterisation of human diaphragm at high strain rate loading. J Mech Behav Biomed Mater **60,** 603, 2016.
65. Engler, A.J., Griffin, M.A., Sen, S., *et al.* Myotubes differentiate optimally on substrates with tissue-like stiffness: pathological implications for soft or stiff microenvironments. J Cell Biol **166,** 877, 2004.
66. Myers, B.S., Woolley, C.T., Slotter, T.L., Garrett, W.E., and Best, T.M. The influence of strain rate on the passive and stimulated engineering stress—large strain behavior of the rabbit tibialis anterior muscle. J Biomech Eng **120,** 126, 1998.
67. Biltz, N.K., Collins, K.H., Shen, K.C., *et al.* Infiltration of intramuscular adipose tissue impairs skeletal muscle contraction. J Physiol **598,** 2669, 2020.
68. Kondash, M.E., Ananthakumar, A., Khodabukus, A., Bursac, N., and Truskey, G.A. Glucose uptake and insulin response in tissue-engineered human skeletal muscle. Tissue Eng Regen Med **17,** 801, 2020.

Address correspondence to:
Christopher R. Rathbone, PhD
Department of Biomedical Engineering
and Chemical Engineering
University of Texas at San Antonio
One UTSA Circle
San Antonio, TX 78249
USA

E-mail: chris.rathbone@utsa.edu

Received: March 18, 2021
Accepted: June 1, 2021
Online Publication Date: August 24, 2021